

# THEORETICAL MODELING OF THE DYNAMICS OF A SEMICONDUCTOR LASER SUBJECT TO DOUBLE-REFLECTOR OPTICAL FEEDBACK

**A. Bakry <sup>a</sup>, S. Abdulrhmann <sup>b,c</sup>, M. Ahmed <sup>d\*</sup>**

<sup>a</sup> Department of Physics, Faculty of Science, King Abdulaziz University, 80203 Jeddah 21589, Saudi Arabia

<sup>b</sup> Department of Physics, Faculty of Sciences, Jazan University, 114 Jazan 22822, Saudi Arabia

<sup>c</sup> Department of Physics, Faculty of Sciences, Assiut University 71516, Assiut, Egypt

<sup>d</sup> Department of Physics, Faculty of Sciences, Minia University 61519, Minia, Egypt

Received August 8, 2015

We theoretically model the dynamics of semiconductor lasers subject to the double-reflector feedback. The proposed model is a new modification of the time-delay rate equations of semiconductor lasers under the optical feedback to account for this type of the double-reflector feedback. We examine the influence of adding the second reflector to dynamical states induced by the single-reflector feedback: periodic oscillations, period doubling, and chaos. Regimes of both short and long external cavities are considered. The present analyses are done using the bifurcation diagram, temporal trajectory, phase portrait, and fast Fourier transform of the laser intensity. We show that adding the second reflector attracts the periodic and period-doubling oscillations, and chaos induced by the first reflector to a route-to-continuous-wave operation. Along this operation, the periodic-oscillation frequency increases with strengthening the optical feedback. We show that the chaos, induced by the double-reflector feedback, is more irregular than that induced by the single-reflector feedback. The power spectrum of this chaos state does not reflect information on the geometry of the optical system, which then has potential for use in chaotic (secure) optical data encryption.

**DOI:** 10.7868/S004445101606002X

## 1. INTRODUCTION

Semiconductor lasers (SLs) have many advantages in comparison to other types of lasers, such as small size, low cost, and the possibility to modulate output power by changing the injected current. Therefore, SLs are key radiation sources in several fields, including fiber-optic communications and optical data processing. In most of their applications, SLs operate in the presence of the external optical feedback (OFB), which is generated due to reflection of laser radiation by an external reflector and re-injection into the laser cavity. The OFB is one of the most studied issues in SLs because it may change the operation dramatically,

inducing various schemes of mode dynamics [1, 2]. The OFB induces chaotic dynamics, which is seen as irregularities in the laser output associated with coherence collapse [3–7]. This effect is pronounced under an intermediate OFB strength and/or long laser-to-reflector distance, and deteriorates the noise level and the SL coherency [2–11].

Most of previous analyses of the SL behavior under the OFB were concerned with reflection of the emitted laser light by a single external reflector. Lang and Kobayashi [12] were a leading group to describe the OFB phenomenon in SLs by including a time-delay term to the rate equation of the electric field. A drawback of this model is its limited application to the regime of weak to moderate strength of the OFB. Later, Abdulrhmann et al. [13] improved this time-delay rate equation model by counting the multiple reflec-

---

\* E-mail: mostafa.farghal@mu.edu.eg

tions in an external cavity and extending the Lang-Kobayashi model to the regime of the strong OFB. This improved model was applied to analyze operation and noise of pumping lasers of fiber amplifiers (Er-doped fibers) [14, 15]. Recently, the model was also applied to explain the resonant modulation response over a millimeter-wave band of SLs operating under the strong OFB [16, 17].

However, in some applications, the SL is subjected to the external OFB from two reflectors. One example is the fiber-optic communication systems in which the laser light is reflected from the near and far end facets of the fiber [18]. Another example is coupling the laser to two external gratings to lock the lasing frequency and increase the emitted power [14]. The double-reflector feedback (DRFB) was also proposed for use in encrypted fiber communication systems to induce chaotic signals that do not carry information on the communication system [19]. The DRFB, however, received inadequate attention in previous modeling on SLs under the OFB [20, 21], which focused on the changes induced in the chaotic state.

In this paper, we extend the time-delay rate equation model of SLs under the single-reflector feedback (SRFB) in [13] to the case of the DRFB and investigate the possible state of laser dynamics. The proposed model is a new contribution to the issue of the OFB in SLs and their applications in optoelectronics. We treat the DRFB as the time delay of laser radiation due to a round trip in each of the two external cavities. The model is applicable to SLs oscillating in single longitudinal modes, such as distributed-feedback (DFB) lasers or even nearly single-mode SLs in which the side-mode suppression ratio exceeds 20 dB [22]. The operation characteristics and dynamics of the laser are classified in terms of the bifurcation diagram of the output power and the phase portrait in addition to the power spectrum of the fast Fourier transform (FFT) of the laser signal. We consider two lengths of the external cavity to characterize the two distinct regimes of short and long external cavities. In both cases, the first reflector is set 3 cm behind the front facet of the laser. This configuration corresponds to the regime of a short external cavity and the laser is attracted to a period-doubling route to chaos with an increase in the SRFB strength. Along this route, the laser changes its operation from continuous waves (CW) to periodic and period-doubling oscillations and ends with chaotic dynamics. We show that when the second cavity is short, the laser is attracted from each of the dynamical states under the SRFB to a route to CW operation with an increase in the DRFB. This route to CW operation is a mirror

to the corresponding route from CW to the corresponding dynamical state under the SRFB. In contrast to the SRFB, the oscillation frequency of the laser along the branch of periodic doubling of the bifurcation diagram increases with an increase in the DRFB. On the other hand, for a long external cavity, the increase in the DRFB attracts the laser to a route to chaos. The DRFB results in smooth chaotic power spectra with two weak and broad peaks around the frequencies of 3.38 and 6.3 GHz. These frequencies have no specific relation and are not sub- or higher harmonics of the resonance frequency of the external cavity. Therefore, this type of chaos has good potential for use in chaotic (secure) optical data encryption.

In the next section, we present the theory of laser dynamics under the DRFB. In Sec. 3, we introduce the procedures of numerical calculations. In Sec. 4, we present the obtained results for both short and long external cavities. Finally, the conclusions appear in Sec. 5.

## 2. TIME-DELAY MODEL OF A SEMICONDUCTOR LASER UNDER THE DRFB

The present model of SLs under the DRFB is schematically illustrated in Fig. 1. The laser diode has a resonance cavity of length  $L_D$  and refractive index  $n_D$ , and is assumed to oscillate in a single longitudinal mode. The light emitted from the front facet of the laser is assumed to travel a round trip in the external cavity 1 formed between the laser and reflector 1 of a power reflectivity  $R_{ex1} < 1$ , and then reflected back to the laser diode. The amount of reflected light and the light injected into the laser cavity from the front facet is determined by the coupling efficiency  $\eta$ . The

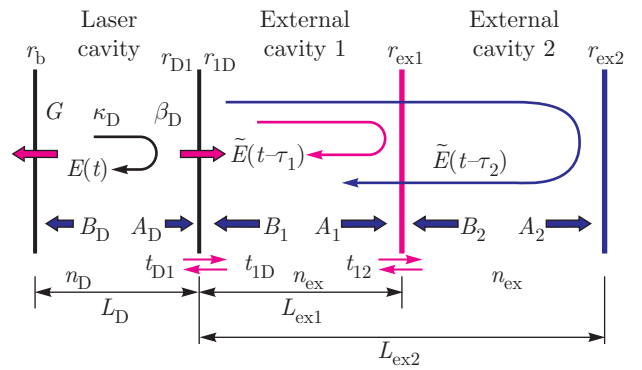


**Fig. 1.** Scheme of a laser diode under the DRFB

round-trip time is determined by the length  $L_{ex1}$  and the refractive index  $n_{ex}$  of the external cavity 1 as

$$\tau_1 = \frac{2n_{ex}L_{ex1}}{c}. \quad (1)$$

Due to the partial reflectivity of reflector 1, the laser radiation in external cavity 1 is transmitted into external cavity 2 formed between reflectors 1 and 2. This radiation then travels a round trip in external cavity 2, during which it is reflected back by reflector 2 and transmitted back into external cavity 1 and then adds to the radiation injected back into the laser cavity. The period of this round trip time is then given by

$$\tau_2 = \frac{2n_{ex}L_{ex2}}{c}, \quad (2)$$

where  $L_{ex2}$  is the length of the external cavity 2. Hence, there are time delays  $\tau_1$  and  $\tau_2$  between the light reflected back from the laser facet into the laser cavity and the light injected back from external reflectors 1 and 2. The electric components of the optical fields in the laser cavity, and the external cavities along the  $z$ -direction are assumed be given by

$$E_D(z, t) = [A_D(z, t) + B_D(z, t)] e^{-i\omega t} + \text{c.c.}, \quad (3)$$

$$0 \leq z \leq L_D,$$

$$E_1(z, t) = [A_1(z, t) + B_1(z, t)] e^{-i\omega t} + \text{c.c.}, \quad (4)$$

$$L_D \leq z \leq L_D + L_{ex1},$$

$$E_2(z, t) = [A_2(z, t) + B_2(z, t)] e^{-i\omega t} + \text{c.c.}, \quad (5)$$

$$L_D + L_{ex1} \leq z \leq L_D + L_{ex2},$$

where  $A_D$ ,  $A_1$ , and  $A_2$  are the forward traveling components of the fields, and  $B_D$ ,  $B_1$ , and  $B_2$  are the backward traveling components.

In the present time-delay model, the DRFB is counted as a time delay of the laser light at the front facet due to the round trips in external two cavities, 1 and 2. Therefore, the boundary conditions at the back facet and front facet are (see Appendix)

$$A_D(0, t) = r_b B_D(0, t), \quad (6)$$

$$B_D(L_D, t) = r_{D1} U A_D(L_D, t), \quad (7)$$

where  $r_b$  and  $r_{D1}$  are the reflection coefficients at the back and front facets,  $U$  is a DRFB function determined by the power reflectivities  $R_f$  at the front facet,  $R_{ex1}$  at the first reflector, and  $R_{ex2}$  at the second reflector,

$$U = 1 - K_{ex1} \frac{A_D(L_D, t - \tau_1)}{A_D(L_D, t)} e^{-i\psi_1} -$$

$$- K_{ex2} \frac{A_D(L_D, t - \tau_2)}{A_D(L_D, t)} e^{-i\psi_2} \equiv |U| e^{-i\varphi}, \quad (8)$$

where the coefficients  $K_{ex1}$  and  $K_{ex2}$  determine the strengths of the OFB from respective reflectors 1 and 2 and are given by

$$K_{ex1} = \eta(1 - R_f) \sqrt{\frac{R_{ex1}}{R_f}}, \quad (9)$$

$$K_{ex2} = \eta(1 - R_f)(1 - R_{ex1}) \sqrt{\frac{R_{ex2}}{R_f}}. \quad (10)$$

Also,  $\psi_1$  and  $\psi_2$  are combined phase terms given by

$$\psi_1 = \varphi_{1D} + \varphi_{ex1} + \omega\tau_1, \quad (11)$$

$$\psi_2 = \varphi_{1D} + \varphi_{ex2} + \omega\tau_2 \quad (12)$$

(for details, see Appendix). The last terms,  $\omega\tau_1$  and  $\omega\tau_2$ , correspond to the time-delay phase changes due to the round trips of light in external cavities 1 and 2, where  $\omega$  is the angular frequency of the laser emission.

By substituting the definitions of the forward and backward components of the field in the laser cavity,

$$A_D(z, t) = A_D(0, t) \exp \{(g - \kappa)z/2 - i\beta z\}, \quad (13)$$

$$B_D(z, t) = B_D(L_D, t) \times$$

$$\times \exp \{(g_D - \kappa_D)(L_D - z)/2 - i\beta_D(L_D - z)\} \quad (14)$$

with  $g_D$ ,  $\kappa_D$ , and  $\beta_D$  as the gain coefficient, the internal loss, and the propagation constant in the laser cavity, respectively, we can write the oscillation condition of the lasers under the DRFB as

$$\sqrt{R_f R_b} |U| \exp \{(g_D - \kappa_D)L_D\} \times$$

$$\times \exp \{-i(2\beta_D L_D + \phi_{D1} + \phi_b + \varphi)\} = 1 \quad (15)$$

( $R_b$  is a the power reflectivity at the back facet) which is then separated into the gain and phase conditions

$$G_{th} = G_{thD} - \frac{c}{n_D L_D} \ln |U|, \quad (16)$$

$$2\beta_D L_D + \phi_{D1} + \phi_b + \varphi = 2q\pi, \quad (17)$$

where  $q$  is an integer and

$$G_{thD} = \frac{c}{n_D} \left( \kappa_D + \frac{1}{2L} \ln \frac{1}{R_f R_b} \right) \quad (18)$$

is the threshold gain in a solitary laser (without the OFB), where  $\kappa_D$  is the material loss in the active region. Equation (16) accounts for variation of the threshold gain of the laser diode due to the OFB, which is responsible for the complexity in the laser dynamics.

We let  $E(z, t)$  denote the electric field in the laser cavity, which is a time-harmonic field characterized by a slowly time-varying amplitude  $\tilde{E}(t)$  as

$$E(r, t) = \tilde{E}(t)\Phi(r)e^{i\omega t} + \text{c.c.}, \quad (19)$$

where  $\Phi(r)$  is the spatial distribution of the field, whose value is normalized in the laser cavity. By substituting this expression in Maxwell's equations, the following rate equation of  $E(t)$  is obtained [23]:

$$\frac{d\tilde{E}}{dt} = \frac{1}{2} \left[ G + i\alpha \frac{a\xi}{V} (N - N_g) - G_{th} \right] \tilde{E}, \quad (20)$$

where  $G$  is the optical gain whose slope with the variation in the injected carrier number  $N$  is  $a$ ,  $G_{th}$  is the threshold gain,  $\xi$  is the confection factor of the field in the active region whose volume is  $V$ ,  $N_g$  is the carrier number at transparency, and  $\alpha$  is the linewidth enhancement factor. The second term describes the phase variation by stimulated emission, which represents the imaginary part of the susceptibility, and is determined with the injected electron number  $N$  based on the third-order approach using the density-matrix analysis developed in [23]. In this approach, the injected density of electrons is determined by the zeroth-order terms of the density matrix in the conduction and valence bands.

The DRFB function  $U$  in Eq. (8) is then rewritten as

$$U = 1 - K_{ex1} \frac{\tilde{E}(t - \tau_1)}{\tilde{E}(t)} e^{-i\psi_1} - K_{ex2} \frac{\tilde{E}(t - \tau_2)}{\tilde{E}(t)} e^{-i\psi_2}. \quad (21)$$

Rate Eq. (20) can be transformed into a couple of equations for the photon number  $S(t)$  contained in the lasing mode and the phase  $\theta(t)$  by writing the complex field amplitude with the phase term as

$$\tilde{E}(t) = \tilde{E}(t) e^{i\theta(t)} \quad (22)$$

with  $S(t)$  being determined from  $\tilde{E}(t)$  as [23]

$$S(t) = \frac{2\varepsilon}{\hbar\omega} |\tilde{E}(t)|^2, \quad (23)$$

where  $\varepsilon$  is the electric permittivity in the active region. Therefore, the following rate equations are obtained:

$$\frac{dS}{dt} = \frac{1}{2} (G - G_{th}) S + C \frac{N}{\tau_s}, \quad (24)$$

$$\frac{d\theta}{dt} = \frac{1}{2} \alpha \frac{a\xi}{V} (N - \bar{N}) - \frac{c}{n_D L_D} \varphi, \quad (25)$$

which, together with the rate equation for  $N$ ,

$$\frac{dN}{dt} = \frac{I}{e} - \frac{N}{\tau_s} - \frac{a\xi}{V} (N - N_g) S, \quad (26)$$

describe the laser dynamics ( $\bar{N}$  is the dc value of the electron number). The optical gain  $G$  is defined including the gain suppression as

$$G = \frac{a\xi}{V} (N - N_g) - BS, \quad (27)$$

where  $B$  is the gain suppression coefficient. In the above equations,  $I$  is the injection current and  $\tau_s$  is the electron lifetime due to spontaneous emission,  $e$  is the electron charge. The term  $CN/\tau_s$  is added to Eq. (24) to account for spontaneous emission with  $C$  being the spontaneous emission factor, which measured the ratio of spontaneous emission included in the lasing action. When the SL is injected far above the threshold, the spontaneous emission factor can be approximated as  $C \approx a\xi\tau_s/V$  [23]. On the other hand, fluctuations in the intensity and phase due to spontaneous emission are commonly described in the rate equations by the Langevin noise sources, which are important to consider when analyzing the noise issue [11]. These sources are dropped in the present model to gain insight into the stable and unstable dynamics of the laser induced by the OFB.

Finally, the OFB function  $U$  in Eq. (21) is written in terms of  $S(t)$  and  $\theta(t)$  as

$$U = 1 - K_{ex1} \sqrt{\frac{S(t - \tau_1)}{S(t)}} \times \exp \{i[\theta(t - \tau_1) - \theta(t) - \psi_1]\} - K_{ex2} \sqrt{\frac{S(t - \tau_2)}{S(t)}} \exp \{i[\theta(t - \tau_2) - \theta(t) - i\psi_2]\}. \quad (28)$$

In this case, the terms  $\exp \{i[\theta(t - \tau_1) - \theta(t)]\}$  and  $\exp \{i[\theta(t - \tau_2) - \theta(t)]\}$  represent the deviations in the optical phase due to chirping induced by the time delay in respective external cavities 1 and 2.

It is worth noting that, for simplicity, the present model does not take into account the multiple reflections inside external cavities, which would add to the complexity of the model. Therefore, the present analysis is applicable to the regimes of the weak and moderate OFB, which include various types of laser dynamics including chaos under the DRFB, whose analysis is the main purpose of this paper. Inclusion of these multiple reflections is critical in the cases of SLs with the strong OFB. Examples include SLs with antireflecting coated facets used as pumping sources in fiber-grating

lasers [14], and SLs with high-reflecting external mirrors used in radio over fiber links to enhance the modulation bandwidth and/or induce the high-frequency resonance modulation [16, 17].

### 3. NUMERICAL CALCULATIONS

The laser dynamics under the DRFB are simulated by numerical integration of rate equations (24)–(26) with the fourth-order Runge–Kutta method. The laser system of AlGaAs emitting in the wavelength of 780 nm is considered in the simulation. Typical numerical values of this laser are listed in Table. The corresponding threshold gain is  $G_{thD} = 2.82 \cdot 10^{11} \text{ s}^{-1}$ , and the threshold current is  $I_{thD} = 22.5 \text{ mA}$ . The external cavity 1 is assumed to have the length  $L_{ex1} = 3 \text{ cm}$ , whereas two lengths of the external cavity 2 are chosen as  $L_{ex2} = 3.5 \text{ cm}$  (short cavity) and  $L_{ex2} = 10 \text{ cm}$  (long cavity). These external cavities are filled with air with the refractive index  $n_{ex} = 1$ . Therefore, the frequency separations of the external-cavity resonance are  $f_{ex1} = 1/\tau_1 = 5 \text{ GHz}$  and  $f_{ex2} = 1/\tau_2 = 4.286 \text{ GHz}$ . The dynamics are examined using the OFB coefficients  $K_{ex1}$  and  $K_{ex2}$  as parameters. The time step of integration was set as 5 ps, which is so small that the cutoff frequency of the FFT of the laser signal is much higher than both the relaxation frequency  $f_r$  of the laser and the resonance frequencies  $f_{ex1}$  and  $f_{ex2}$  of the external cavities. The integration was carried out over the period  $T = 3\text{--}5 \mu\text{s}$  for which the operation reaches a steady state. The SL is assumed to operate far above the threshold,  $I = 2.0I_{thD}$ , to minimize the contribution of spontaneous emission to the lasing action. The phases  $\psi_1$  and  $\psi_2$  are arbitrary and set to correspond to the respective time-delay phases  $\omega\tau_1$  and  $\omega\tau_2$ . The phase  $\varphi$  of the feedback light is determined as

$$\varphi = \arctan \frac{\text{Im } U}{\text{Re } U} + p\pi, \quad (29)$$

where  $p$  is an integer and is chosen to vary continuously for the time evolution, because the solution of arctangent is limited to the range from  $-\pi/2$  to  $+\pi/2$  in the computer work.

The dc values  $\bar{S}$  and  $\bar{N}$  of the photon number and the electron number are determined from the steady-state solutions of the solitary rate equations as

$$\bar{S} = \frac{I - I_{thD}}{eG_{thD}}, \quad (30)$$

$$\bar{N} = \frac{N_{thD} + VB\bar{S}/a\xi}{\bar{S} + 1}, \quad (31)$$

where  $N_{thD}$  is the electron number at the threshold.

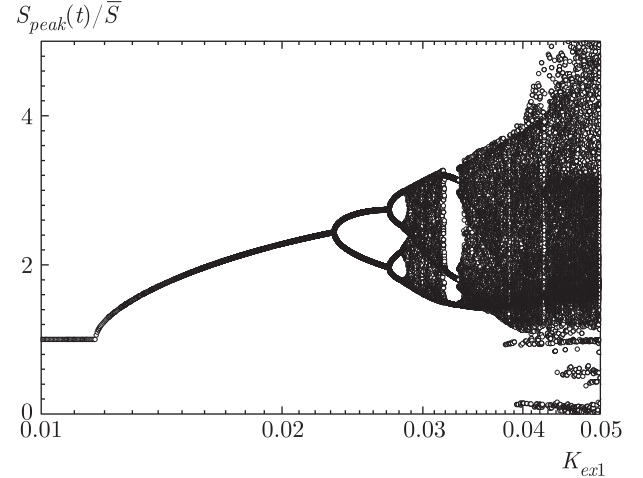


**Fig. 2.** Bifurcation diagram of laser dynamics under the SRFB with  $L_{ex1} = 3 \text{ cm}$

### 4. RESULTS AND DISCUSSIONS

First, we present the various states of laser dynamics induced by the SRFB. The influence of the DRFB on the laser dynamics is then illustrated by including the second reflector and examining the variations occurring in each dynamical state of the SRFB.

#### 4.1. Laser dynamics under the SRFB

The dynamics of the SL induced by the first reflector is examined by means of the bifurcation diagram in Fig. 2 of the temporal peak value of the photon number  $S_{peak}(t)$  versus the OFB coefficient  $K_{ex1}$ . These peak values  $S_{peak}(t)$  are normalized by the average photon number  $\bar{S}$  at the corresponding value of  $K_{ex1}$ . Figure 2 indicates that the laser keeps the CW operation of a solitary laser for sufficiently small values of  $K_{ex1}$ . When  $K_{ex1}$  increases beyond the Hopf-bifurcation point  $K_{ex1} = 0.0117$ , the relaxation oscillations of the laser become undamped and the laser is characterized by a periodic-oscillation output. These oscillations are of the 1-period and continue up to  $K_{ex1} = 0.023$ , beyond which the periodic oscillation is divided into two branches, indicating generation of period-doubling oscillations. When  $K_{ex1} > 0.0286$ , the oscillation period divides further and shows a tour and then chaotic dynamics. The chaotic dynamics ends when  $K_{ex1} = 0.032$ . The shown period-doubling route to chaos characterizes the SL coupled to a short external cavity with  $f_{ex}/f_r > 1.43$  (or  $f_r/f_{ex} > 0.7$ ) [9, 24].

Examples of the induced states of laser dynamics due to the SRFB are shown in Fig. 3: a periodic oscil-

**Table.** Values of the parameters of 780-nm AlGaAs lasers and system configurations used in calculations

Parameter	Value	Unit
Tangential coefficient of gain, $a$	$2.75 \cdot 10^{-12}$	$\text{m}^3 \cdot \text{s}^{-1}$
Electron number at transparency, $N_g$	$3.15 \cdot 10^8$	—
Nonlinear gain coefficient, $B_c$	$6.19 \cdot 10^{-5}$	$\text{s}^{-1}$
Electron number characterizing $B$ , $N_s$	$2.55 \cdot 10^8$	—
Electron life time, $\tau_s$	2.79	ns
Spontaneous emission factor $C$	$10^{-5}$	—
Linewidth enhancement factor, $\alpha$	2	—
Refractive index of active region, $n_D$	3.59	—
Length of the active region, $L_D$	300	$\mu\text{m}$
Volume of the active region, $V$	150	$\mu\text{m}^3$
Field confinement factor, $\xi$	0.2	—
Reflectivity at front facet, $R_f$	0.3	—
Reflectivity at back facet, $R_b$	0.8	—

lation ( $K_{ex1} = 0.02$ ), period doubling ( $K_{ex1} = 0.025$ ), and chaos ( $K_{ex1} = 0.04$ ). Figures 3a–3c plot the temporal variations of  $S(t)$ , Figs. 3g–3i depict the phase portrait of  $S(t)$  versus  $N(t)$ , and Figs. 3d–3f plot the power spectra of the laser output calculated by means of the FFT of  $S(t)$ . As found from Fig. 3a, the laser shows a uniform periodic oscillation with frequency  $f_{PO} = 3.325$  GHz, which is comparable to the relaxation frequency  $f_r$ . The phase portrait in Fig. 3g indicates a limit-cycle attractor characterizing the periodic oscillation. The power spectrum in Fig. 3d reflects the periodic oscillation by the sharp peak at  $f = 3.325$  GHz and weaker peaks at higher harmonics. It is worth examining the variation of the frequency  $f_{PO}$  with the OFB strength  $K_{ex1}$  along the periodic-oscillation branch in Fig. 2. The results are plotted in Fig. 4, which shows that  $f_{PO}$  decreases from 3.32 to 3.2 GHz with an increase in  $K_{ex1}$ . This effect is also predicted in [9] for fiber-grating lasers.

The period-doubling oscillation is seen in Fig. 3b as  $S(t)$  has periodic oscillations with two peaks of different heights in every two successive periods, and the phase portrait in Fig. 3h indicates a double-loop attractor. The power spectrum in Fig. 3e is characterized by sharp peaks at  $f = 3.2$  GHz and  $f/2$  as well as weaker peaks at the higher harmonics of these two frequencies.

The chaotic operation is characterized by the irregular time pattern of  $S(t)$  shown in Fig. 3c, and the phase portrait in Fig. 3i corresponds to a chaotic attractor. The power spectrum in Fig. 3f reveals three broad and weak peaks, the strongest peak occurs at the frequency  $f_1 = 3.4$  GHz, and the other weaker two peaks occur at frequencies  $f_2 = 4.6$  and  $f_3 = 6.3$  GHz.

## 4.2. Laser dynamics under the DRFB

### 4.2.1. Regime of short cavity ( $L_{ex2} = 3.5$ cm)

We also use the bifurcation diagram to illustrate the variations occurring in the laser dynamics when adding the second reflector. We first assume that the second reflector is set just 0.5 cm behind the reflector 1, making the external cavity 2 operate in the regime of a short external cavity ( $L_{ex2} = 3.5$  cm). Figure 5 plots the bifurcation diagrams when  $K_{ex1}$  is set to correspond to the periodic oscillation ( $K_{ex1} = 0.02$ ), period doubling ( $K_{ex1} = 0.025$ ), and chaos ( $K_{ex1} = 0.04$ ). Interesting features are indicated in each of these states of dynamics: (1) the laser dynamics begins with the dynamical state of the laser under the SRFB in the regime of very small values of  $K_{ex2}$ ; (2) the increase in  $K_{ex2}$  attracts the laser to a route-to-CW operation; and (3) this route-to-CW operation is a mirror to the

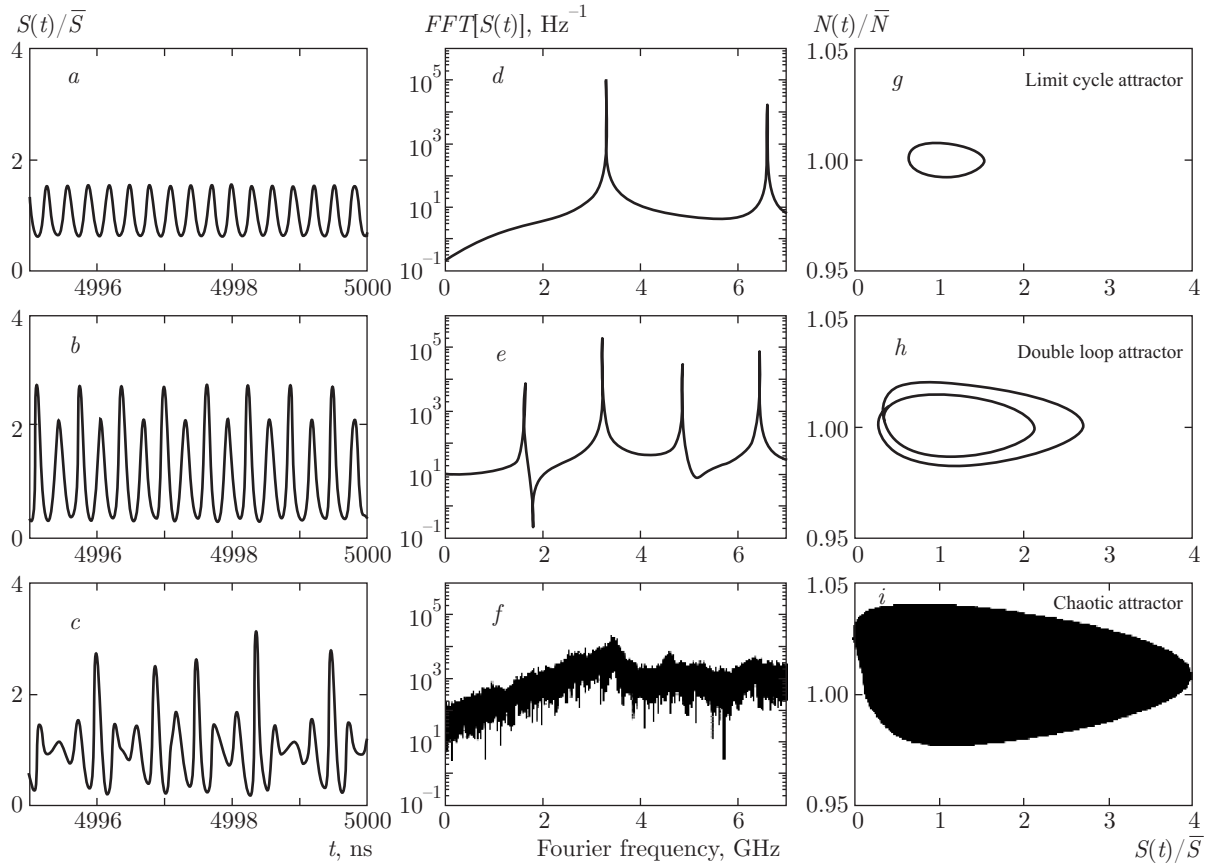


**Fig. 3.** Dynamical states of the SL under the SRFB,  $L_{ex1} = 3.0$  cm: (a) the periodic oscillation with  $K_{ex1} = 0.03$ ; (b) the period doubling with  $K_{ex1} = 0.025$ , and (c) chaos with  $K_{ex1} = 0.04$ ; (d)–(f) power spectra of the laser output; (g)–(i) the phase portrait of  $S(t)$  versus  $N(t)$

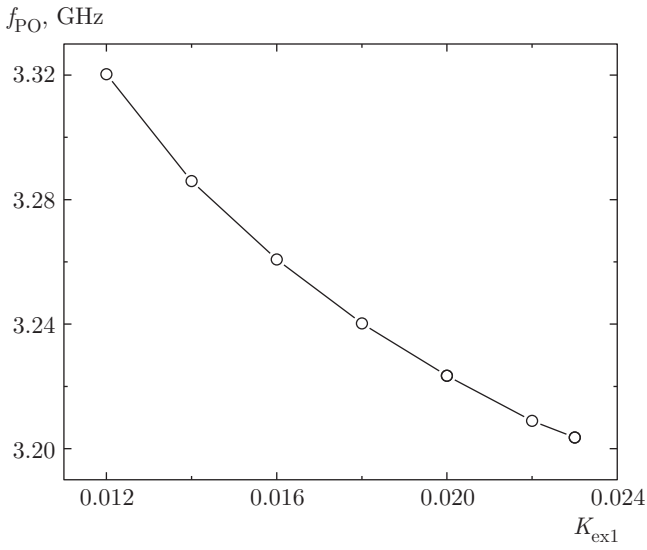


**Fig. 4.** Variation of the periodic-oscillation frequency  $f_{PO}$  with  $K_{ex1}$

corresponding route-from-CW to the relevant dynamical state at this level of  $K_{ex1}$  in the bifurcation diagram in Fig. 2 for the SRFB. That is, the reflector 2 can stabilize the irregular dynamics induced by the SRFB and maintain the CW operation.

It is interesting to show the variation of the periodic-oscillation frequency  $f_{PO}$  along the periodic-oscillation branches in the above bifurcation diagrams. In contrast to the case of the SRFB,  $f_{PO}$  increases with the increase in the OFB strength  $K_{ex2}$ , as shown in Fig. 6. When  $K_{ex1} = 0.02$  (the periodic-oscillation state under the SRFB),  $f_{PO}$  increases from 3.24 to 3.38 GHz; when  $K_{ex1} = 0.025$  (the period-doubling state under the SRFB),  $f_{PO}$  increases from 3.22 to 3.5 GHz; and when  $K_{ex1} = 0.04$  (chaos state under the SRFB),  $f_{PO}$  increases from 3.34 to 3.57 GHz.

We also investigate the spectral characteristics of the chaos state under the DRFB. Figure 7 plots the power spectrum of the laser with chaotic dynamics when  $K_{ex1} = 0.04$  and  $K_{ex2} = 0.005$ . Although the

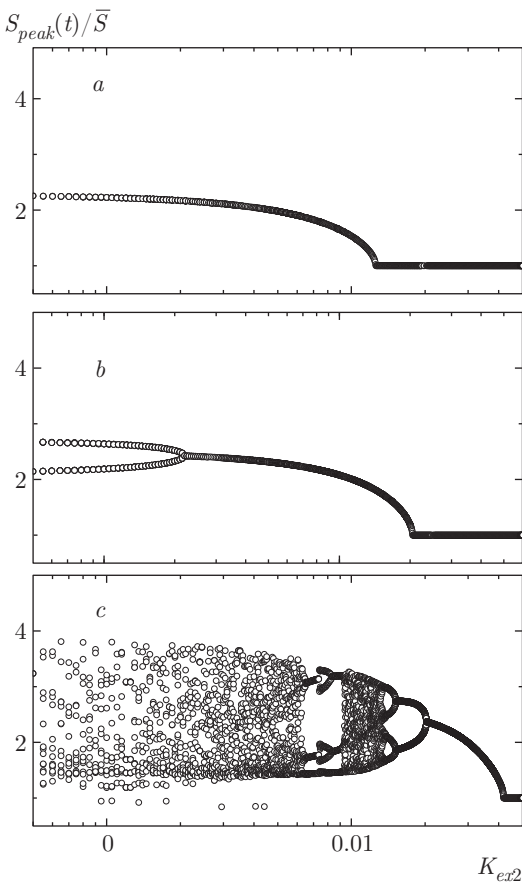


**Fig. 5.** Bifurcation diagrams of laser dynamics under DRFB with  $L_{ex1} = 3$  cm and  $L_{ex2} = 3.5$  cm: (a)  $K_{ex1} = 0.02$ , (b)  $K_{ex1} = 0.025$ , and (c)  $K_{ex1} = 0.04$

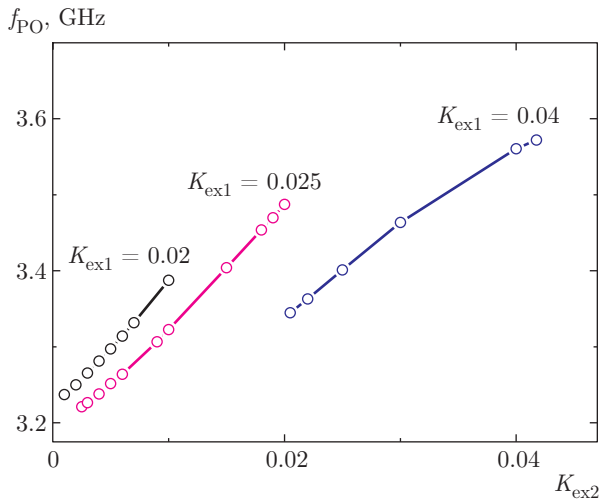


**Fig. 6.** Variation of periodic-oscillation  $f_{PO}$  with  $K_{ex2}$  along the periodic-oscillation branches in Fig. 5 for  $K_{ex1} = 0.02$ ,  $0.025$ ,  $0.04$

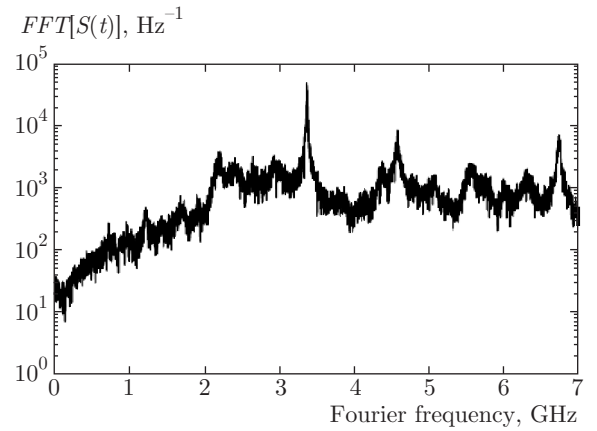


**Fig. 7.** Power spectrum of chaos for  $K_{ex1} = 0.04$  with  $K_{ex2} = 0.005$  ( $L_{ex1} = 3$  cm,  $L_{ex2} = 3.5$  cm)

shown spectrum reveals more enhanced peaks than the spectrum of the chaos state under the SRFB in Fig. 3f, the frequency positions of these peaks have no relationships and their values are random. The frequency of the highest peak is 3.4 GHz, which is the same peak frequency of SRFB.

#### 4.2.2. Regime of long cavity ( $L_{ex2} = 10$ cm)

Here, we assume that the reflector 2 is set 7 cm behind the first reflector, making a long external cavity of the length  $L_{ex2} = 10$  cm. Figure 8 plots the bifurcation diagrams when the SRFB induces the same dynamics as in Fig. 5. We also can see that the laser dynamics begins with the dynamical state of the laser under the SRFB in the regime of a very weak OFB from the reflector 2 (very small values of  $K_{ex2}$ ). However, the increase in  $K_{ex2}$  does not attract the laser to a route-to-CW operation in this case, but attracts it to a route-to-chaos. The range of  $K_{ex2}$  that corresponds to the chaos dynamics is narrowest when  $K_{ex1} = 0.02$ , which corresponds to the periodic oscillation under the SRFB, and widest when  $K_{ex1} = 0.04$ , which corresponds to chaos. Figure 9 plots two examples of the most typical power spectrum of the chaotic dynamics generated under the DRFB for  $K_{ex1} = 0.04$  with  $K_{ex2} = 0.018$  and  $K_{ex1} = 0.029$  with  $K_{ex2} = 0.03$ . Compared with the chaotic power spectra in Figs. 3f and 7, the shown spectra are smoother with the two weaker and broader peaks. The higher peak occurs at a frequency of about 3.8 GHz, which is 400 MHz higher than the pronounced peak in the chaos spectrum of the SRFB in Fig. 3f. The lower peak occurs at a frequency of about 6.3 GHz, which is not related with the frequency of the primary peak. In addition, these two peak frequencies have no

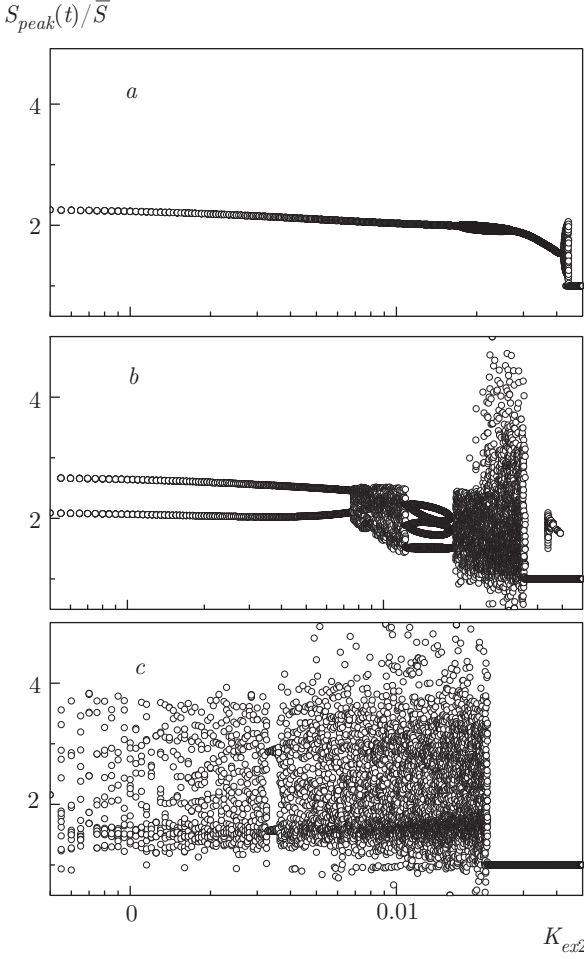


**Fig. 8.** Bifurcation diagrams of laser dynamics under the DRFB with  $L_{ex1} = 3$  cm and  $L_{ex2} = 10$  cm: (a)  $K_{ex1} = 0.02$ , (b)  $K_{ex1} = 0.025$ , and (c)  $K_{ex1} = 0.04$

clear relationships with the resonance frequencies  $f_{ex1}$  and  $f_{ex2}$  of the external cavities. That is, these noise spectra do not carry information on the geometry of the optical system. These characteristics indicate that the power spectrum of the chaos state under the DRFB is more irregular than that characterizing the SRFB. Therefore, the present design of the DRFB can be used to generate chaotic signals applicable in the chaotic (secure) data encryption.

## 5. CONCLUSIONS

We introduced a theoretical model for the dynamics of semiconductor lasers operating under the DRFB by extending our previous improved time-delay rate equation model of the SRFB. The states of laser dynamics were investigated in the regimes of both

short (3.5 cm) and long (10 cm) external cavities. We set the first reflector at 3 cm from the front facet of the laser, which corresponds to a period-doubling route-to-chaos under the SRFB. The results show that along this route, the laser changes its operation from the CW to periodic oscillations followed by period-doubling oscillations and then chaos. The periodic-oscillation frequency decreases from 3.32 to 3.2 GHz with an increase in the SRFB. When the second external cavity is short, the laser is attracted from each of the dynamical states under the SRFB to a route-to-CW operation. This route-to-CW operation is a mirror to the corresponding a route from CW to the corresponding dynamic state under the SRFB. In contrast to the SRFB, the oscillation frequency of the laser along the periodic-oscillation branch of the bifurcation diagram increases with an increase in the DRFB, reaching 3.58 GHz. When the external cavity is long, the increase in the DRFB strength attracts the laser to a route to chaos. Compared with the case of the SRFB, the DRFB results in smoother chaotic power spectra with two weak and broad peaks around the frequencies of 3.38 and 6.3 GHz. These frequencies have no specific relation and are not sub- or higher harmonics of the resonance frequency of the external cavity. This type of chaos has potential applications in chaotic (secure) optical data encryption. The present model concerns with semiconductor lasers oscillating in a single mode, and could be extended to multimode lasers, which would be the subject of future research.

This paper was funded by the Deanship of Scientific Research (DSR), King Abdulaziz University, Jeddah, under the grant № 130-894-D1435. The authors, therefore, gratefully acknowledge the DSR technical and financial support.

## APPENDIX

From the scheme in Fig. 1 of a SL under the DRFB, the boundary conditions at the back and front facets are given as

$$A_D(0, t) = r_b B_D(0, t), \quad (\text{A.1})$$

$$\begin{aligned} B_D(L_D, t) &= r_{D1} A_D(L_D, t) + \\ &+ \eta t_{D1} t_{1D} r_{ex1} A_D(L_D, t - \tau_1) e^{-i\omega\tau_1} + \\ &+ \eta t_{D1} t_{1D} t_{12}^2 r_{ex2} A_D(L_D, t - \tau_2) e^{-i\omega\tau_2} = \\ &= r_{D1} U A_D(L_D, t), \quad (\text{A.2}) \end{aligned}$$

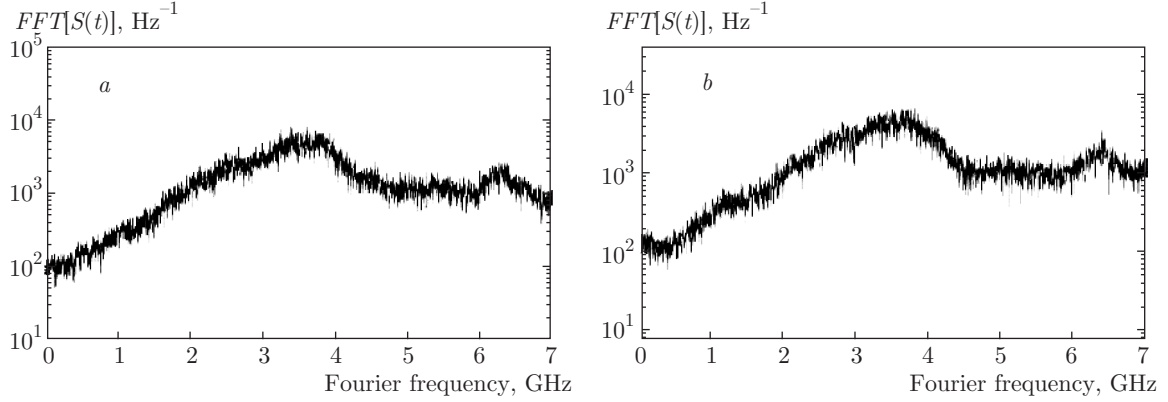


**Fig. 9.** Power spectrum of chaos when  $L_{ex1} = 3$  cm and  $L_{ex2} = 10$  cm: (a)  $K_{ex1} = 0.029$  and  $K_{ex2} = 0.018$ ; (b)  $K_{ex1} = 0.029$  and  $K_{ex2} = 0.03$

where  $U$  is a DRFB function determining the OFB strength due to time delays in external cavities 1 and 2, and is given by

$$U = 1 + \eta \frac{t_{D1} t_{1D}}{r_{D1}} \left[ r_{ex1} \frac{A_D(L_D, t - \tau_1)}{A_D(L_D, t)} e^{-i\omega\tau_1} + r_{ex2} \frac{A_D(L_D, t - \tau_2)}{A_D(L_D, t)} e^{-i\omega\tau_2} \right], \quad (\text{A.3})$$

where  $r_{D1}$  and  $t_{D1}$  are the reflection and transmission coefficients at the front facet from the laser cavity to external cavity 1, and  $r_{1D}$  and  $t_{1D}$  are the reflection and transmission coefficients from external cavity 1 to the laser cavity. Furthermore,  $r_{ex1}$  and  $r_{ex2}$  are the reflection coefficients at reflectors 1 and 2, and  $t_{12}$  is the transmission coefficient at reflector 1;  $r_b$  is the reflection coefficient at the back facet. These transmission and reflection coefficients are complex values in general, and are expressed in terms of the power reflection coefficients  $R_b$ ,  $R_f$ ,  $R_{ex1}$ , and  $R_{ex2}$  and phase changes such as

$$r_{D1} = \sqrt{R_f} \exp(-i\varphi_{D1}), \quad (\text{A.4})$$

$$r_{1D} = \sqrt{R_f} \exp(-i\varphi_{1D}), \quad (\text{A.5})$$

$$r_b = \sqrt{R_b} \exp(-i\varphi_b), \quad (\text{A.6})$$

$$r_{ex1} = \sqrt{R_{ex1}} \exp(-i\varphi_{ex1}), \quad (\text{A.7})$$

$$r_{ex2} = \sqrt{R_{ex2}} \exp(-i\varphi_{ex2}), \quad (\text{A.8})$$

$$t_{D1} = \frac{n_{ex}}{n_D} \sqrt{1 - R_f} \exp(-i\varphi_{tD}), \quad (\text{A.9})$$

$$t_{1D} = \frac{n_D}{n_{ex}} \sqrt{1 - R_f} \exp(-i\varphi_{tD}), \quad (\text{A.10})$$

$$t_{12} = \sqrt{1 - R_{ex1}} \exp(-i\varphi_{t1}) \quad (\text{A.11})$$

with the phase relationships

$$\varphi_{D1} + \varphi_{1D} - 2\varphi_{tD} = \pm\pi. \quad (\text{A.12})$$

By substituting the above expressions in Eq. (A.3), the DRFB relations in Eqs. (8)–(12) are obtained.

## REFERENCES

1. W. W. Tkach and A. R. Chraplyvy, IEEE J. Light-wave Technol. **LT-4**, 1655 (1986).
2. N. Schunk and K. Petermann, IEEE J. Quant. Electron. **24**, 1242 (1988).
3. D. Lenstra, B. H. Verbeek, and A. J. den Boef, IEEE J. Quant. Electron. **21**, 674 (1985).
4. G. C. Dente, P. S. Durkin, K. A. Wilson, and C. E. Moeller, IEEE J. Quant. Electron. **24**, 2441 (1988).
5. J. Sacher, W. Elsasser, and E. O. Gobel, Phys. Rev. Lett. **63**, 2224 (1989).
6. B. Tromborg and J. Mork, IEEE Photon. Technol. Lett. **2**, 549 (1990).
7. J. Mork, J. Mork, and B. Tromborg, Phys. Rev. Lett. **65**, 1999 (1990).
8. S. Abdulrhmann, M. Yamada, and M. Ahmed, Int. J. Num. Model. **24**, 218 (2011).
9. M. Ahmed, M. Yamada, and S. Abdulrhmann, Int. J. Num. Model. **22**, 434 (2009).
10. S. Abdulrhmann, M. Ahmed, and M. Yamada, Proc. SPIE **4986**, 1 (2003).
11. M. Ahmed and M. Yamada, J. Appl. Phys. **95**, 7573 (2004).
12. R. Lang and K. Kobayashi, IEEE J. Quant. Electron. **16**, 347 (1980).

13. S. Abdulrhmann, M. Ahmed, T. Okamoto et al., IEEE J. Selected Topics in Quant. Electron. **9**, 265 (2003).
14. M. Ahmed, S. W. Z. Mahmoud, and M. Yamada, Int. J. Num. Model. **20**, 117 (2007).
15. S. Abdulrhmann, Turk. J. Phys. **36**, 225 (2012).
16. M. Ahmed, A. Bakry, R. Altuwirqi et al., Jpn. J. Appl. Phys. **52**, 124103 (2013).
17. M. Ahmed, A. Bakry, R. Altuwirqi et al., J. Eur. Opt. Soc. **8**, 130064 (2013).
18. G. P. Agrawal and T. M. Shen, J. Lightwave Technol. **4**, 58 (1986).
19. Y. Hong, M. W. Leeand, and K. A. Shore, Proc. SPIE **5614**, 72 (2004).
20. J. G. Wu, G. Q. Xia, and Z. M. Wu, Opt. Express **17**, 20124 (2009).
21. A. Toppens and U. Parlitz, Phys. Rev. E **78**, 016210 (2008).
22. M. Ahmed, Physica D **176**, 212 (2003).
23. M. Yamada, *Theory of Semiconductor Lasers*, Springer, Tokyo (2014), Chs. 6 and 8.
24. M. Ahmed, S. W. Z. Mahmoud, and M. Yamada, Eur. Phys. J. D **41**, 175104 (2012).